

# Electronic structure and optical properties of $(\text{BeTe})_n/(\text{ZnSe})_m$ superlattices

M. CAID<sup>1</sup>, H. RACHED<sup>1</sup>, D. RACHED<sup>1\*</sup>, R. KHENATA<sup>2</sup>, S. BIN OMRAN<sup>3</sup>, D. VASHNEY<sup>4</sup>,  
B. ABIDRI<sup>1</sup>, N. BENKHETTOU<sup>1</sup>, A. CHAHED<sup>5</sup>, O. BENHELLAL<sup>5</sup>

<sup>1</sup>Laboratoire des Matériaux Magnétiques, Faculté des Sciences, Université Djillali Liabès de Sidi Bel-Abbès,  
Sidi Bel-Abbès 22000, Algeria

<sup>2</sup>Laboratoire de Physique Quantique et de Modélisation Mathématique (LPQ3M), Département de Technologie,  
Université de Mascara, 29000, Algeria

<sup>3</sup>Department of Physics and Astronomy, College of Science, King Saud University,  
P.O. Box 2455, Riyadh 11451, Saudi Arabia

<sup>4</sup>Materials Science Laboratory, School of Physics, Vigyan Bhavan, Devi Ahilya University,  
Khandwa Road Campus, Indore 452001, India

<sup>5</sup>Condensed Matter and sustainable development Laboratory (LMCDD), University of Sidi Bel-Abbes,  
Sidi Bel-Abbes 22000, Algeria

The structural, electronic and optical properties of  $(\text{BeTe})_n/(\text{ZnSe})_m$  superlattices have been computationally evaluated for different configurations with  $m = n$  and  $m \neq n$  using the full-potential linear muffin-tin method. The exchange and correlation potentials are treated by the local density approximation (LDA). The ground state properties of  $(\text{BeTe})_n/(\text{ZnSe})_m$  binary compounds are determined and compared with the available data. It is found that the superlattice band gaps vary depending on the layers used. The optical constants, including the dielectric function  $\epsilon(\omega)$ , the refractive index  $n(\omega)$  and the refractivity  $R(\omega)$ , are calculated for radiation energies up to 35 eV.

Keywords: *FP-LMTO; electronic structure; optical properties; superlattices*

© Wrocław University of Technology.

## 1. Introduction

Recently, efforts have been made to distinguish semiconductor materials that are useful in scientific applications, as well as their relevant intrinsic properties. Semiconductors are used in a variety of remarkable device applications. Superlattices have been made available for use in many applications owing to developments in their production techniques, such as the strain-induced lateral ordering process [1, 2], molecular beam epitaxy [2, 3] and low-pressure chemical-vapor deposition [2, 4]. The development of superlattices is actively being researched by studying the properties of superlattices with reduced size and dimensionality and by understanding their properties within the context

of designing new electronic and optoelectronics devices.

Superlattices (SLs) are structures that are made up of two types of semiconducting (s.c) materials, with one type (s.c<sub>1</sub>) acting as a quantum well and the other (s.c<sub>2</sub>) acting as a quantum barrier [2]. In the present work, we explore the structural and electronic properties of the II-VI semiconductor compounds BeTe and ZnSe. The most widely studied telluride/selenide superlattice (SL) structures are ZnTe/ZnSe and ZnSe/BeTe [5].

The objective of the present work is to extract physical parameters from the structural and electronic properties of  $(\text{BeTe})_n/(\text{ZnSe})_m$  superlattices (where  $n$  and  $m$  are numbers of monolayers;  $n = 1, 2, 3, 4$ , or  $5$ ;  $m = 1, 2, 3, 4$ , or  $5$ ) and to compare them with previous theoretical and experimental results. We seek to more carefully and accurately

\*E-mail: rachdj@yahoo.fr

assess the effects of different superlattice configurations on electronic properties and, in particular, to observe the dependence of band gap behavior on the layers used.

We thus investigate the structural and electronic properties of nine  $(\text{BeTe})_n/(\text{ZnSe})_m$  superlattices with a tetragonal structure by using the full-potential linear muffin-tin orbital (FP-LMTO) method in the framework of density functional theory (DFT) within the local density approximation (LDA) for the exchange correlation functional. The organization of the present study is as follows: the adopted computational method is discussed in Section 2, the results are presented and discussed in Section 3, and conclusions and brief remarks are given in Section 4.

## 2. Details of calculation

Density functional theory (DFT) is a powerful tool that is widely employed for the calculation of electronic and structural properties of solids and has been shown to yield relevant information about condensed matter phases and materials worth computing. In this work, the FP-LMTO method as implemented in the LmtART computer code [6, 7] was applied to perform first-principles total-energy calculations. This method is based on DFT, which is a universal quantum mechanical approach for many-body problems. In this approach, the quantum many-body problem of an interacting electron gas is mapped exactly onto a set of single particles moving in an effective local potential with the same density as the real system; the obtained one-electron equations are called the Kohn-Sham equations [8, 9].

In the LMTO method, space is divided into an interstitial region (IR) and non-overlapping muffin-tin (MT) spheres centered at the atomic sites. In the IR regions, the basis set consists of plane waves. Inside the MT spheres, the basis sets are described by radial solutions of the one-particle Schrödinger equation (at fixed energy), and their energy derivatives are multiplied by spherical harmonics. We have used the recently developed LmtART package (LmtART 7) with the electrons

exchange-correlation energy described using the Perdew-Wang parameterization of the local density approximation (LDA) [10].

The details of the calculations are as follows: the charge density and the potential are represented inside the muffin-tin sphere (MTS) spherical harmonics up to  $l_{\text{max}} = 6$ . The  $k$  integration over the Brillouin zone is performed using the tetrahedron method [11] and is set up differently following the case. For  $\text{SL}(m, n)$ , meshes of (6, 6, 6), (8, 8, 8) and (10, 10, 10) are utilized for  $m + n = 2$ ,  $m + 2 = 4$  and  $m + n = 6$ , respectively. The self-consistent calculations are considered to be converged within  $10^{-6}$  for the total energy. The values of the sphere radii (MTS) and the number of plane waves (NPLW) used in the present calculations are listed in Table 1. We observed that NPLW does not vary with  $n + m$ ; by contrast, the RMTS and  $E_{\text{cut}}$  vary with different configurations of the layers.

## 3. Results and discussion

### 3.1. Structural properties

Electronic configuration of superlattices  $(\text{BeTe})_n/(\text{ZnSe})_m$  in the ground state is  $\text{Be}:[\text{He}] 2s^2$ ,  $\text{Te}:[\text{Kr}] 4d^{10} 5s^2 5p^4$ ,  $\text{Zn}:[\text{Ar}] 3d^{10} 4s^2$  and  $\text{Te}:[\text{Se}] 4d^{10} 4p^4 4s^2$ . As a first step, we determined the structural properties of the binary compounds in the zinc-blende (ZB) structure. The lattice constant ( $a_0$ ) was obtained by fitting the total energy as a function of volume to Birch's [12] equation of state. We obtained the lattice constant, the bulk modulus and its pressure derivative from this numerical fitting procedure. The calculated structural parameters of binary compounds for LDA are presented in Table 2, along with the previous theoretical calculations and experimental data. Inspection of Table 2 shows that our LDA results are in reasonable agreement with experimental and available theoretical values. In the second step, we were interested in the quantum well superlattice consisting of binary compounds. In our case, (ZnSe) played the role of the barrier while (BeTe) acted as the well.

In the present work, the superlattices consist of a sequence of alternating  $n$  and  $m$  layers

Table 1. Input parameters: number of plane waves, energy cut-off and muffin-tin radii.

Compounds	NPLW (Total)	$E_{\text{cut}}$ [Ryd]	MTS [a.u.]			
			Be	Te	Zn	Se
$(\text{BeTe})_1/(\text{ZnSe})_1$	16242	137.1748	2.122	2.476	2.122	2.476
$(\text{BeTe})_2/(\text{ZnSe})_2$	32458	137.0922	2.024	2.526	2.165	2.392
$(\text{BeTe})_3/(\text{ZnSe})_3$	48690	137.6625	2.020	2.540	2.158	2.401
$(\text{BeTe})_1/(\text{ZnSe})_3$	32458	137.0651	2.123	2.477	2.180	2.392
$(\text{BeTe})_3/(\text{ZnSe})_1$	32458	137.3635	2.022	2.540	2.121	2.474
$(\text{BeTe})_2/(\text{ZnSe})_4$	48690	137.3247	2.022	2.528	2.172	2.401
$(\text{BeTe})_4/(\text{ZnSe})_2$	48690	137.6141	2.020	2.546	2.140	2.431
$(\text{BeTe})_1/(\text{ZnSe})_5$	48690	137.0638	2.123	2.477	2.182	2.401
$(\text{BeTe})_5/(\text{ZnSe})_1$	48690	138.0711	2.017	2.548	2.108	2.475

of ZnSe and BeTe along a specified growth direction. X-axis as the growth axis and superlattice  $(m, n)$  with tetragonal symmetry have been chosen ( $n$  is the number of ZnSe monolayers, and  $m$  is the number of BeTe monolayers). The superlattice SL(1,1) is made up of alternate monolayers of BeTe and ZnSe, each monolayer containing two atoms; this alternation increases with  $m$  and  $n$ . The elementary cell volume is proportional to the number of monolayers. For the considered structures, we have performed structural optimization of the parameter of the host compound by minimizing the total energy with respect to the cell parameters. The total energies calculated as a function of the unit cell volume are fitted to the Birch-Murnaghan equation of state [12].

The deduced results are illustrated in Table 3. The data show that the SL11 lattice parameter interpolates the bulk material values, giving a good epitaxial interface and minimizing the creation of defects; for the other SL with  $m = n$ , the lattice parameter increases with the number of layers used. Finally, for  $n \neq m$ , we observe a slight difference of the lattice parameter, especially when the number of BeTe layers increases. This difference is due to the atomic radius of the compound, which causes compression of the superlattice.

### 3.2. Electronic properties

For the binary compounds and their superlattices, the electronic band structures have been calculated at the equilibrium lattice. The most

prominent features of the calculated band gaps are shown in Table 2 and Table 4. It is interesting to note that BeTe has an indirect band gap with the valence band maximum at  $\Gamma$  and conduction band minimum at X, whereas ZnSe has a direct band gap with the valence band maximum (VBM) and conduction band minimum (CBM) at  $\Gamma$ . The calculated band gaps for the binary compounds are in good agreement with the available theoretical results. We can see also that, due to the approximations used in our work, the band gap values are underestimated compared with the experimental data.

In Fig. 1 and Fig. 2, we show the calculations of band structures for superlattices at  $m = n$  and  $m \neq n$ . Examination of these figures shows that they exhibit both types of band gaps: for  $m = n$  superlattices there is a direct band gap at  $\Gamma$  whereas for  $m > n$ , the superlattice band gap is indirect, with VBM located at  $\Gamma$  and CBM at R (except for  $m = 4$  and  $n = 2$ , where the gap is direct but is close to  $\Gamma$ -R). The values of these gaps are 1.427 and 2.10 eV, respectively. No previous superlattice results are available for comparison; from the binary compound data, we conclude that the underestimation of band gaps by LDA also applies to superlattices. This underestimation is due to strongly correlated 3d electrons of Zn.

To describe the number of states that are available to be occupied by electrons per interval of energy at each energy level, we have also calculated the total and the partial densities of states (DOS) of these compounds, as displayed in Fig. 3 and Fig. 4.

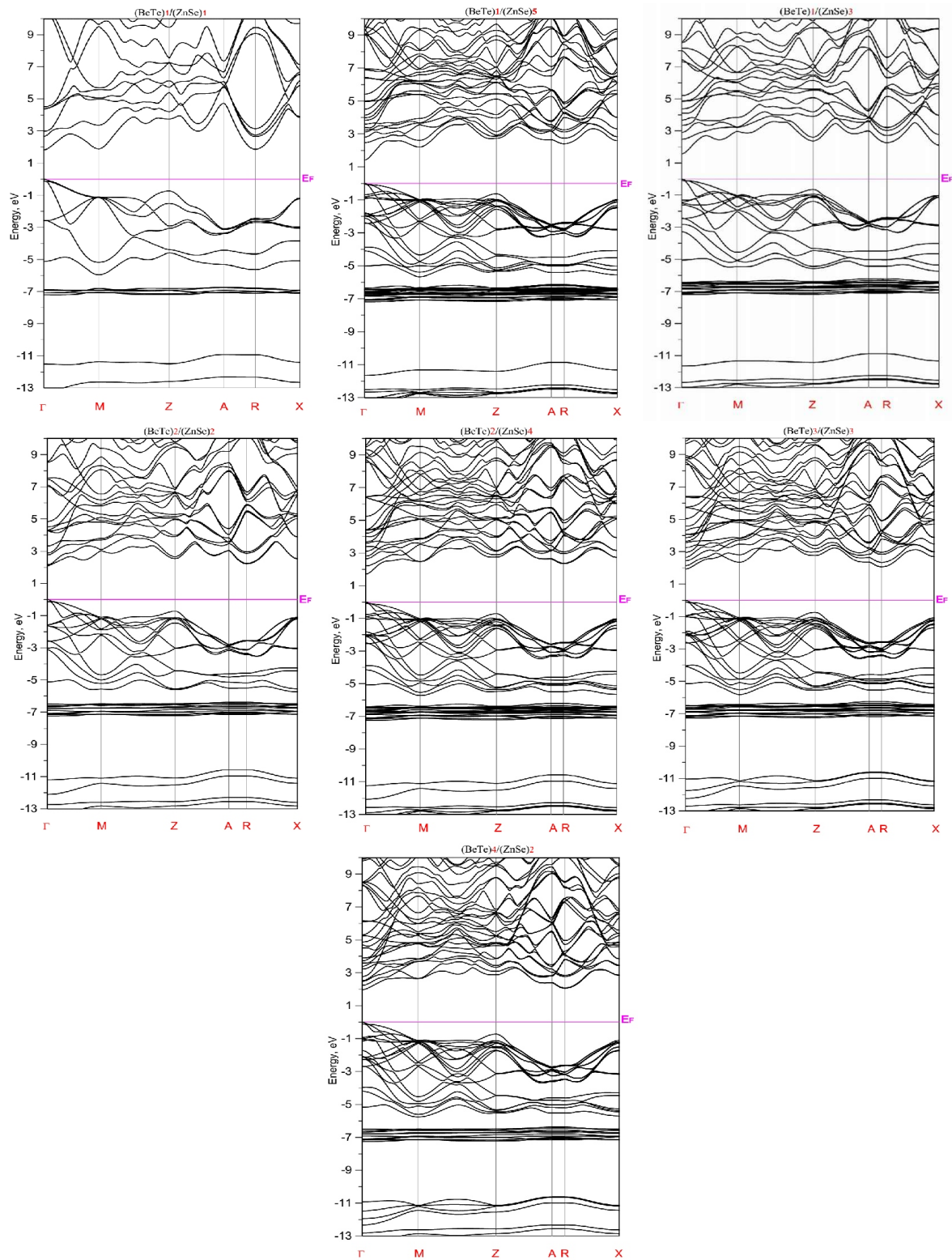


Fig. 1. Band structure along the symmetry lines of the Brillouin zone for  $(\text{BeTe})_n/(\text{ZnSe})_m$  superlattices at direct band gap.

Table 2. Calculated lattice parameter  $a$  (Å), bulk modulus  $B_0$  (GPa), derived modulus  $B'_0$  and gap energy  $E_g$  (eV) for the binary compounds at equilibrium volume.

This work	Lattice constant (Å)		Bulk modulus $B_0$ (GPa)		$B'_0$		$E_g$ (eV)			
	Exp	Other works	This work	Exp	This work	Exp	This work	Exp ( $\Gamma$ -X)	Other works	
BeTe	5.588	5.617 <sup>a</sup> , 5.581 <sup>b</sup> , 5.58 <sup>c</sup> , 5.53 <sup>d</sup> , 5.556 <sup>e</sup> , 5.531 <sup>f</sup> , 5.556 <sup>g</sup>	56.448	66.8 <sup>h</sup> , 62.36 <sup>b</sup> , 60 <sup>c</sup> , 71 <sup>d</sup> , 55 <sup>e</sup> , 71 <sup>f</sup> , 64.90 <sup>g</sup>	3.62	4 <sup>a</sup>	3.69 <sup>b</sup> , 3.72 <sup>c</sup> , 3.38 <sup>d</sup> , 3.56 <sup>e</sup> , 3.377 <sup>f</sup> , 3.40 <sup>g</sup>	1.907	2.7 <sup>h</sup>	1.76 <sup>g</sup> , 1.8 <sup>d</sup>
ZnSe	5.65	5.667 <sup>i,j</sup> , 5.624 <sup>k</sup> , 5.618 <sup>l</sup> , 5.666 <sup>m</sup> , 5.666 <sup>n</sup> , 5.578 <sup>o</sup> , 5.611 <sup>p</sup>	59.68	64.7 <sup>i</sup> , 71.82 <sup>k</sup> , 67.6 <sup>l</sup> , 67.32 <sup>m</sup> , 62.45 <sup>n</sup> , 71.84 <sup>o</sup> , 75.20 <sup>p</sup>	3.96	4.77 <sup>i</sup>	4.88 <sup>k</sup> , 4.67 <sup>l</sup> , 4.05 <sup>n</sup> , 5.99 <sup>o</sup> , 4.57 <sup>p</sup>	1.0963	2.82 <sup>q</sup>	1.31 <sup>k</sup> , 1.863 <sup>r</sup> , 1.83 <sup>s</sup>

<sup>a</sup>[13], <sup>b</sup>[14], <sup>c</sup>[15], <sup>d</sup>[16], <sup>e</sup>[17], <sup>f</sup>[18], <sup>g</sup>[19], <sup>h</sup>[20], <sup>i</sup>[21], <sup>j</sup>[22], <sup>k</sup>[23], <sup>l</sup>[24], <sup>m</sup>[25], <sup>n</sup>[27], <sup>o</sup>[28], <sup>p</sup>[29], <sup>q</sup>[30], <sup>r</sup>[30], <sup>s</sup>[31].

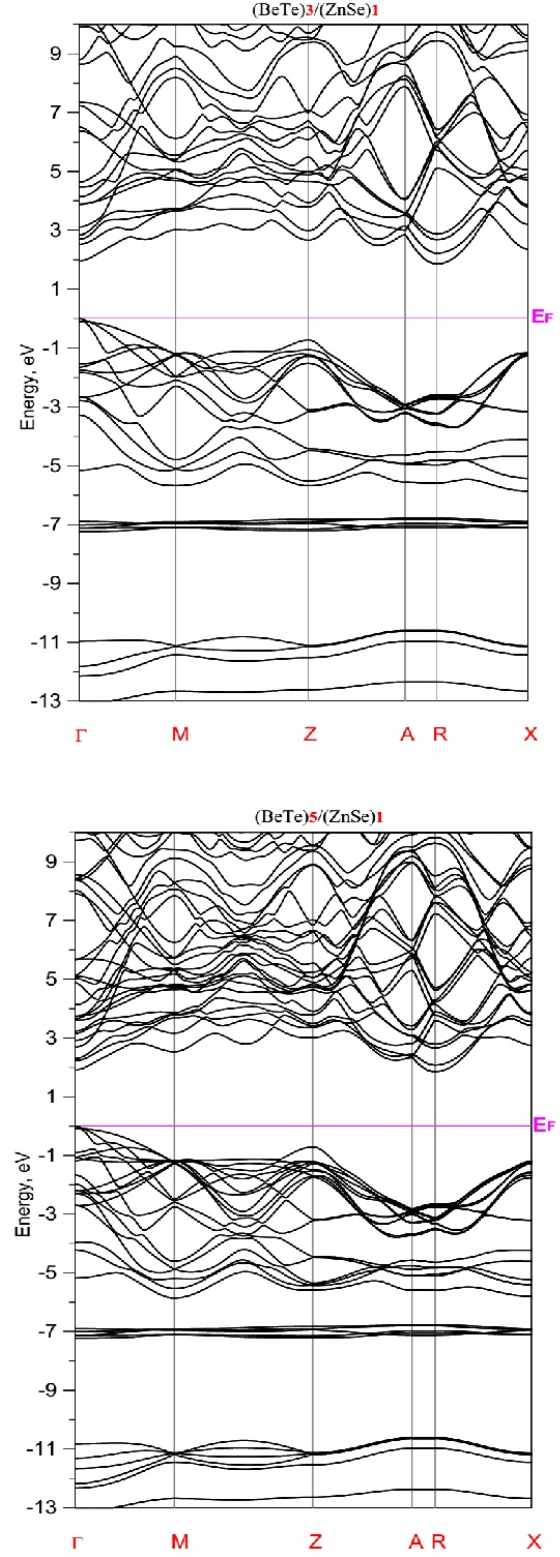


Fig. 2. Band structure along the symmetry lines of the Brillouin zone for  $(\text{BeTe})_n/(\text{ZnSe})_m$  superlattices at indirect band gap.

Table 3. The calculated equilibrium constant  $a$  (Å), bulk modulus  $B_0$  (GPa) and  $B'_0$  for superlattices  $(\text{BeTe})_n/(\text{ZnSe})_m$ .

Compounds	$a$ (Å)	$B_0$ (GPa)	$B'_0$
$(\text{BeTe})_1/(\text{ZnSe})_1$	5.619	58.947	4.99803
$(\text{BeTe})_2/(\text{ZnSe})_2$	11.241	59.829	4.14331
$(\text{BeTe})_3/(\text{ZnSe})_3$	16.826	62.328	4.16186
$(\text{BeTe})_1/(\text{ZnSe})_3$	11.242	64.827	4.93767
$(\text{BeTe})_3/(\text{ZnSe})_1$	11.230	60.270	3.47019
$(\text{BeTe})_2/(\text{ZnSe})_4$	16.847	64.97	4.38255
$(\text{BeTe})_4/(\text{ZnSe})_2$	16.830	61.299	3.17126
$(\text{BeTe})_1/(\text{ZnSe})_5$	16.863	65.856	4.64635
$(\text{BeTe})_5/(\text{ZnSe})_1$	16.802	58.065	3.36946

Table 4. Calculated energy band gaps.

Compounds	$E_g$ (eV)	Nature
$(\text{BeTe})_1/(\text{ZnSe})_1$	1.829038	Gap direct
$(\text{BeTe})_2/(\text{ZnSe})_2$	2.102459	Gap direct
$(\text{BeTe})_3/(\text{ZnSe})_3$	1.933643	Gap direct
$(\text{BeTe})_1/(\text{ZnSe})_3$	1.582407	Gap direct
$(\text{BeTe})_3/(\text{ZnSe})_1$	1.858339	Gap indirect
$(\text{BeTe})_2/(\text{ZnSe})_4$	1.706723	Gap direct
$(\text{BeTe})_4/(\text{ZnSe})_2$	1.971915	Gap direct
$(\text{BeTe})_1/(\text{ZnSe})_5$	1.427891	Gap direct
$(\text{BeTe})_5/(\text{ZnSe})_1$	1.852561	Gap indirect

Inspection of Fig. 3 shows that there are differences in the conduction band densities of states of the two binary compounds, with 3 regions present in the ZnSe DOS and two regions present in the BeTe DOS. This difference is due to the existence of the middle region dominated by the 3d-Zn states of the ZnSe compound; by contrast, the Be d states are empty for the BeTe compound.

Examination of Fig. 4 shows that the topology of the superlattices densities of states is the same as that of the ZnSe binary compound. Two examples are shown in Fig. 4:  $m = n = 1, 2, 3$  and  $m \neq n$  with  $m = 3$  and  $n = 1$ . The lower occupied bands, located between  $\sim -13$  and  $-10.8$  eV, are primarily formed by the Se 4s and Be 2s states, with small contributions by the Zn 4s/4p/3d states. The states in the middle region between  $\sim -7$  and  $-6$  eV occur mainly because of the Zn 3d states, with small

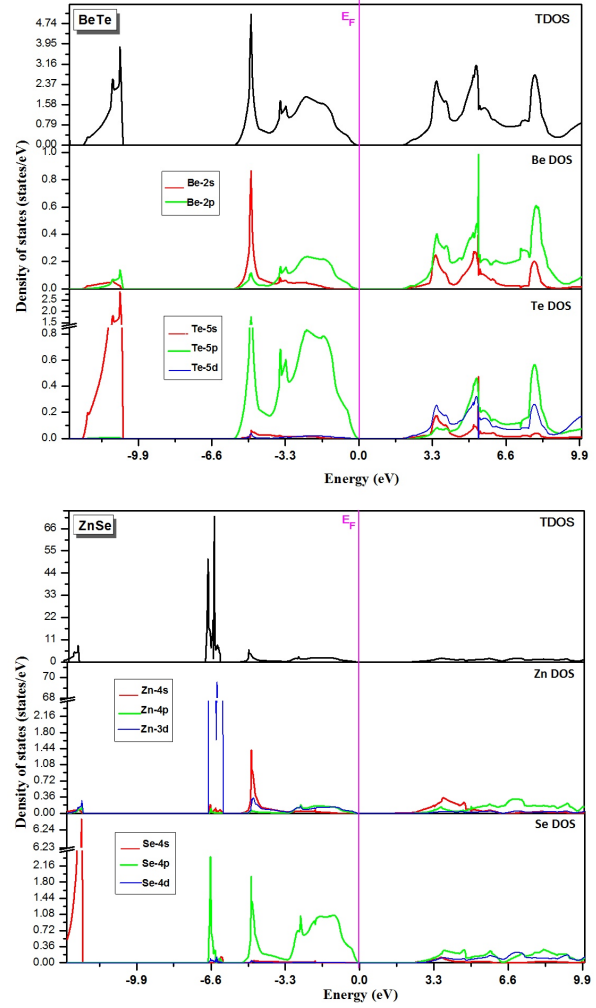


Fig. 3. Total and partial density of states (DOS) for BeTe and ZnSe compounds.

contributions due to the other Se and Zn states and the Te 5p/5d states. The states in the last region between  $\sim 5.8$  eV and the Fermi level are dominated by the Te 5p and Se 4p states. Hybridization between these states is apparent in this region. In the conduction band, the dominant contribution to the band structure from 2 to 10 eV varies depending on the relative contributions of the states of all the elements, with strong hybridizations between the Te 5p and Te 5d states, as well as the Se 4p and Se 4d states.

### 3.3. Optical properties

In this section, we discuss the optical properties of a material that must be investigated to

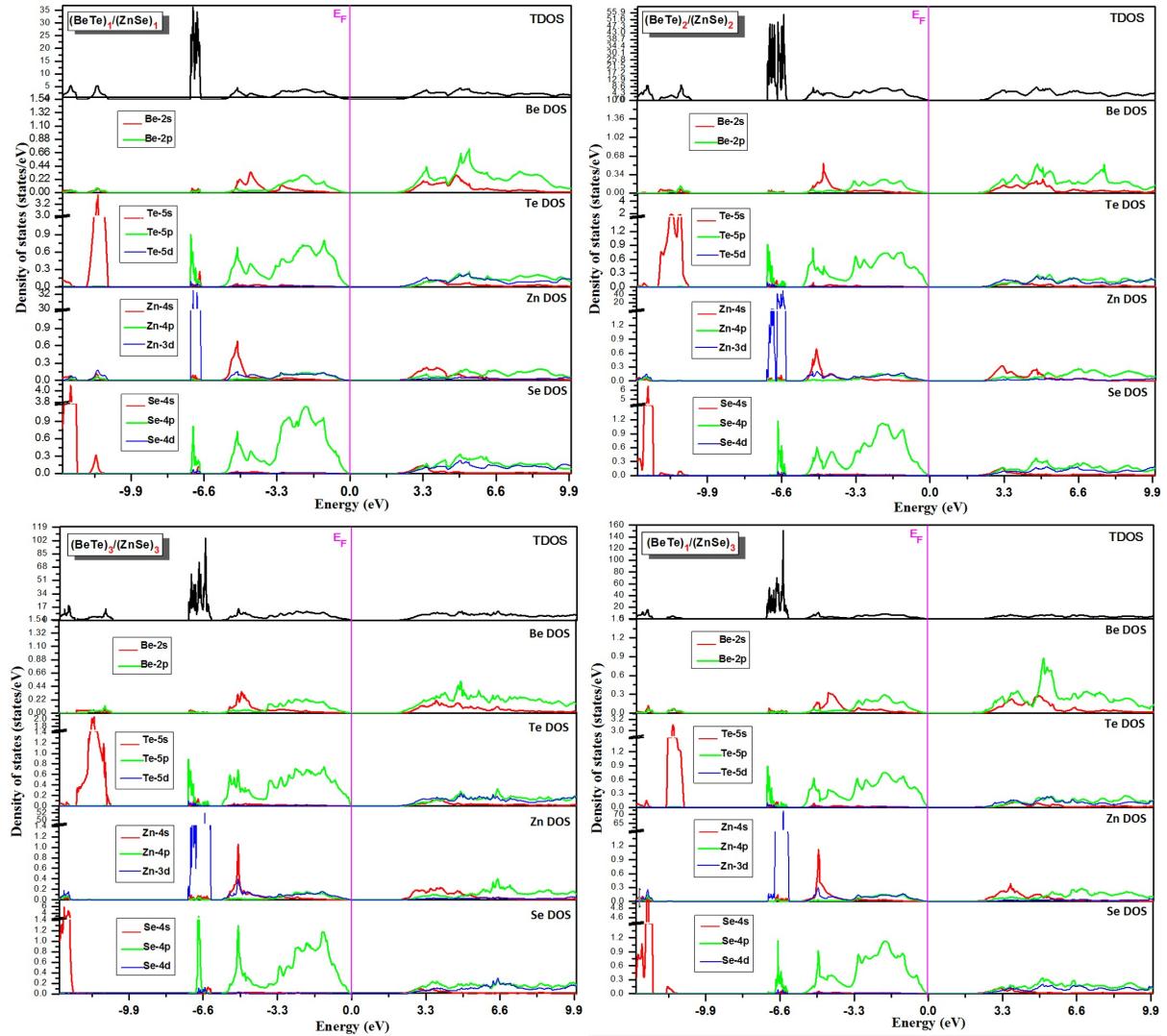


Fig. 4. Total and partial density of states (DOS) for  $(\text{BeTe})_n/(\text{ZnSe})_m$  superlattices with  $n = m = 1, 3$  and  $n \neq m$  (1, 3).

determine its potential usefulness in optoelectronic applications. For this reason, we only chose the materials that showed a direct band gap character in our LDA study. When examining the optical response of the compounds under investigation, it is convenient to take into account the transitions of electrons from the occupied energy bands to the unoccupied energy bands, particularly at the high symmetry points in the Brillouin zone. The real part  $\epsilon_1(\omega)$  of the dielectric function can be determined from the imaginary part  $\epsilon_2(\omega)$  by the Kramers-Kronig relationship. A fully detailed description of the calculation of the optical properties

was presented previously by Ambrosch-Draxl and Sofo [32].

To calculate the optical spectra of the dielectric function,  $\epsilon(\omega)$ , a dense mesh of uniformly distributed  $k$ -points is required. Hence, the Brillouin zone integration was performed with 400  $k$ -points in the irreducible part of the Brillouin zone for SL(1, 1), SL(2, 2), SL(3, 3), SL(1, 3), SL(2, 4), SL(4, 2), and SL(1, 5) without broadening. Using the optical relationships described above, we have calculated the real and imaginary components of the frequency dielectric function and then used

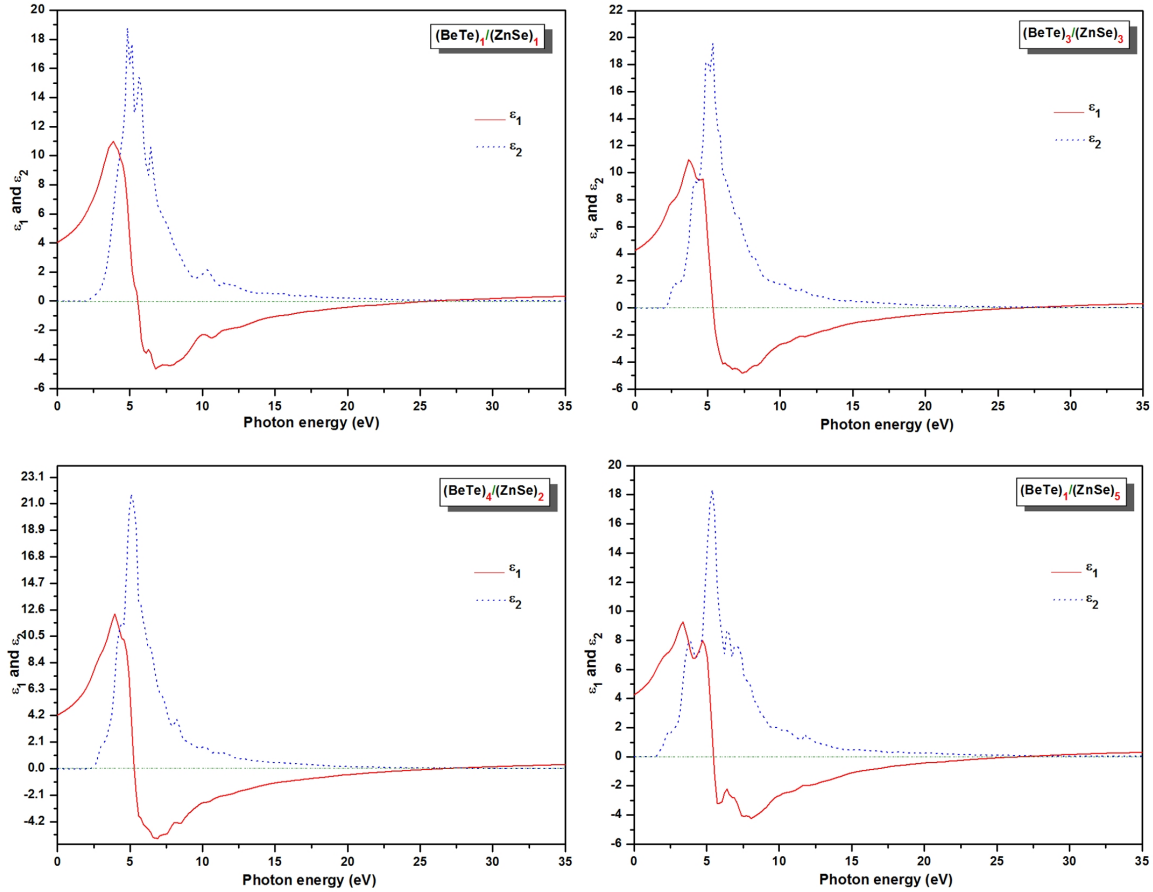


Fig. 5. Calculated dielectric functions (real and imaginary) for  $(\text{BeTe})_n/(\text{ZnSe})_n$  superlattices at direct band gap.

these functions to determine the refractive index  $n(\omega)$  and reflectivity  $R(\omega)$ . Due to the similarities of the topology of the optical properties of SLs, in Fig. 5 we only present the real and imaginary parts of  $\epsilon(\omega)$  for SL(1, 1), SL(3, 3), SL(4, 2) and SL(1, 5).

To illustrate a minor difference in the description of these properties, the dielectric function  $\epsilon_2(\omega)$  exhibits a structure that varies depending on the composition of the superlattice; thus, we can see that the  $\epsilon_2(\omega)$  peaks depend on the ZnSe compound layers. The threshold for direct optical transitions for the  $\Gamma$ - $\Gamma$  band gap is between the valence band maximum and the conduction band minimum. Beyond these thresholds, the  $\epsilon_2(\omega)$  curve rises rapidly because the number of the points contributing to  $\epsilon_2(\omega)$  increases abruptly. The main peaks in the spectra are located

between 4.82 and 5.73 eV. The real part  $\epsilon_1(\omega)$  of the frequency-dependent dielectric function was obtained according to the Kramers-Kronig dispersion relation and is displayed in Fig. 5. We note that peak intensities in these spectra typically occur between 3.86 and 3.96 eV, i.e. between the peaks of the binary compounds located at 3.334 and 4.38 eV for ZnSe and BeTe, respectively. Subsequently,  $\epsilon_1(\omega)$  becomes negative between 6.75 and 8.06 eV, depending on the superlattice configuration.

In Fig. 6 and Fig. 7, the refractive index  $n(\omega)$  and the reflectivity spectrum  $R(\omega)$  are plotted for several different superlattices (SL(1, 1), SL(3, 3), SL(4, 2) and SL(1, 5)). The optical spectra of the superlattices are similar. From our examination of the reflectivity spectra of the superlattices, we note that  $R(\omega)$  increases by up to 70 % and then starts

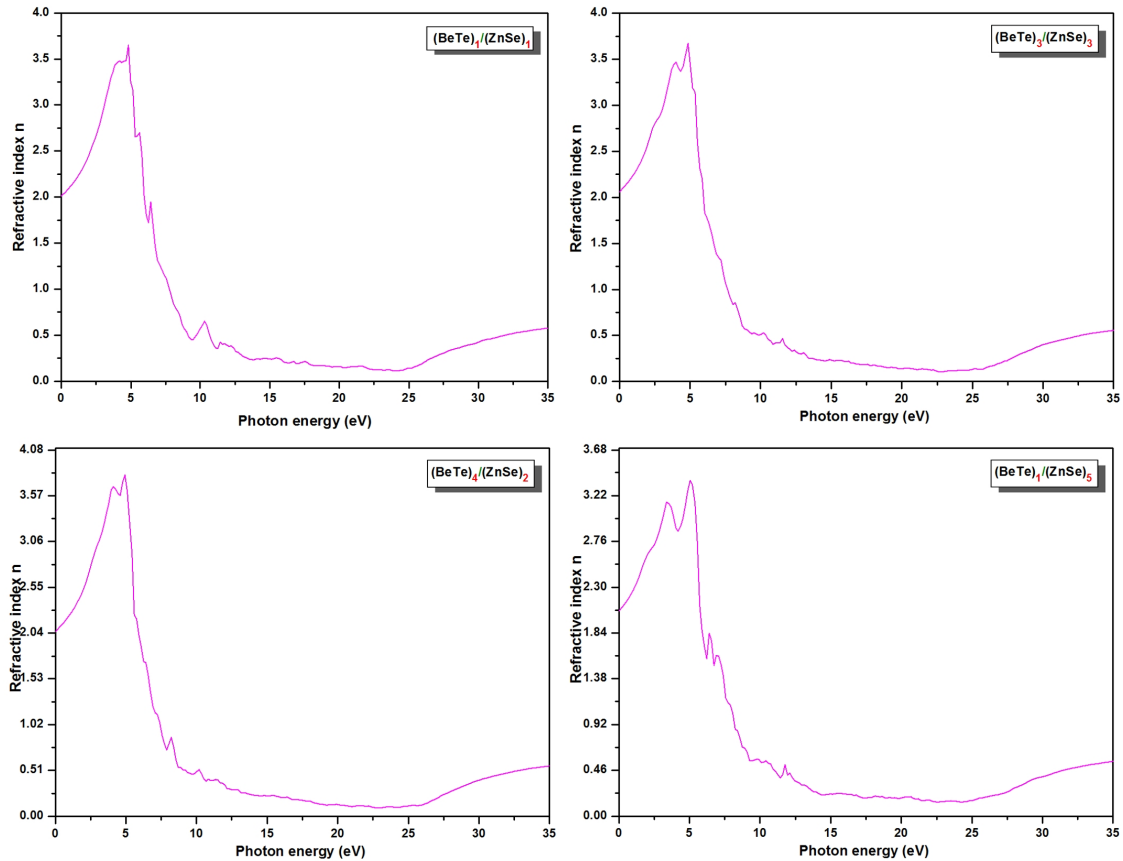


Fig. 6. Calculated refractive index  $n(\omega)$  for  $(\text{BeTe})_n/(\text{ZnSe})_n$  superlattices at direct band gap.

to decrease at approximately 26 eV. This result suggests that these superlattices behave like semiconductors. The static dielectric constant  $\epsilon_1(0)$  is given by the low energy limit of  $\epsilon_1(\omega)$ . Note that we do not include the phonon contributions to dielectric screening, and  $\epsilon_1(0)$  corresponds to the static dielectric constant of  $\sim 2.01$ . To our knowledge, there are no available experimental or theoretical results for the optical properties of these superlattices, so the present work can be considered to be a predictive study.

## 4. Conclusions

We have performed detailed investigation on the structural, elastic, electronic, and optical properties of  $(\text{BeTe})_n/(\text{ZnSe})_m$  superlattices using the full-potential linear muffin-tin orbital method within the Perdew-Wang LDA. The calculated

ground-state properties of binary compounds are in good agreement with the available experimental data. Our results for band structure and DOS show that our superlattices are semiconductors, but their band gaps change from direct to indirect ( $\Gamma$ - $\Gamma$  to  $\Gamma$ -R) depending on the configuration of the layers. The results obtained for the energy band gaps using LDA show a strong dependence on the number of layers used. The imaginary and real parts of the dielectric function were investigated and analyzed to identify the optical transitions. The static dielectric constants  $\epsilon(0)$  and refractivity  $R(\omega)$  were calculated. Finally, because the maximum reflectivities of the  $(\text{BeTe})_n/(\text{ZnSe})_m$  superlattice compounds are in the ultra-violet region, these materials can potentially be used in ultra-violet radiation shielding.

## Acknowledgements

The authors (Khenata and Bin-Omran) acknowledge the financial support provided by the Deanship of the Scientific

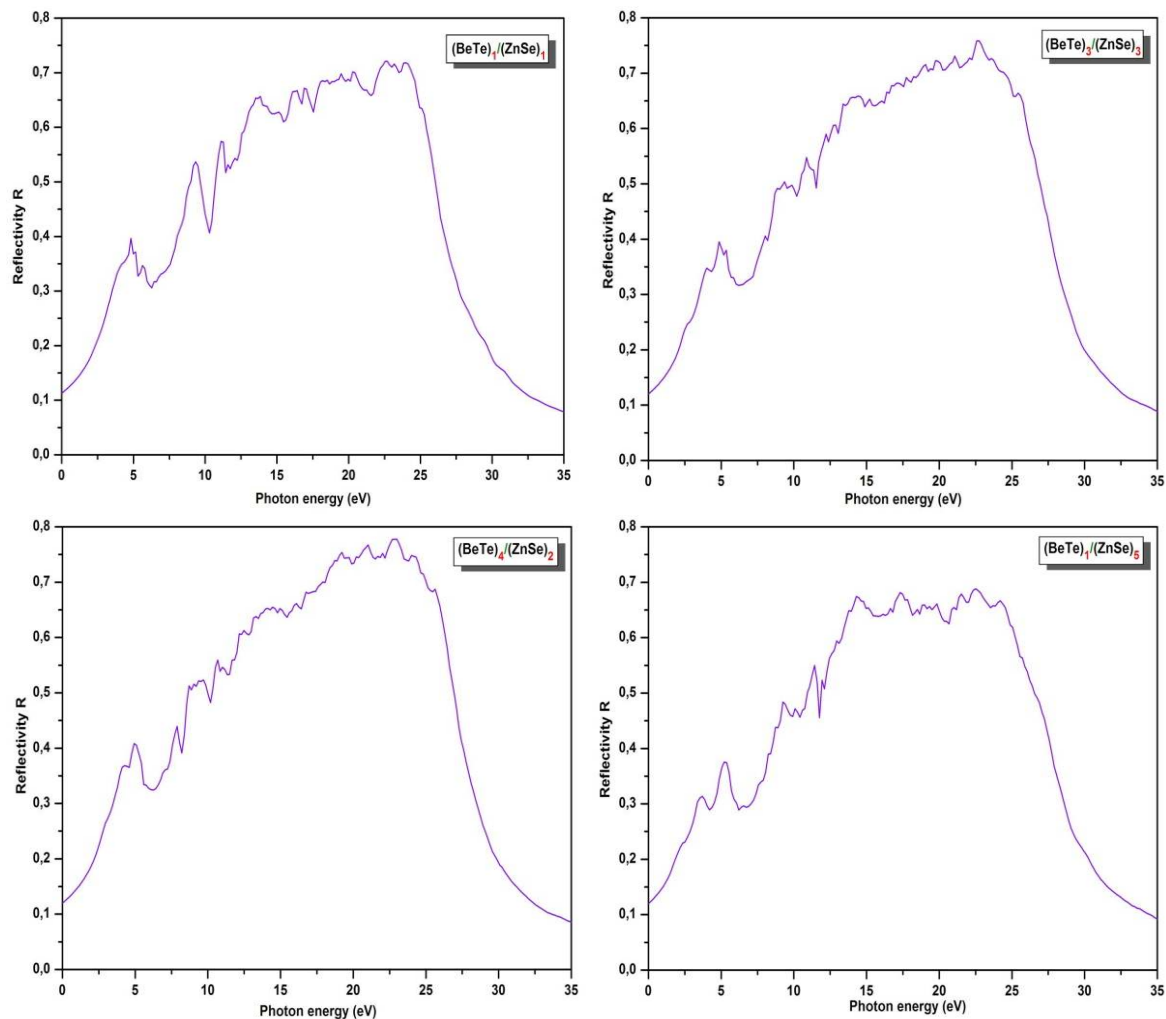


Fig. 7. Calculated reflectivity  $R(w)$  for  $(\text{BeTe})_n/(\text{ZnSe})_n$  superlattices at direct band gap.

Research at the King Saud University for funding this work through Research Group Project No.: RPG-VPP-088.

## References

- [1] MASCARENHAS A., ALONSO R.G., HORNER G.S., FROYEN S., HSIEH K.C., CHENG K.Y., *Phys. Rev. B*, 48 (1993), 4907.
- [2] MERABET M., RACHED D., KHENATA R., BENALIA S., ABIDRI B., BETTAHAR N., BIN OMRAN S., *Physica B*, 406 (2011), 3247.
- [3] CAPASSO F., MARGARITONODO G. (Eds.), *Heterojunctions Band Discontinuities. Physics and Devices Applications*, Amsterdam, North-Holland, 1987.
- [4] ANGUS C., HAYMAN C.C., *Science*, 241 (1988), 877.
- [5] ZAITSEV S.V., YAKOVLEV D.R., WAAG A., *Fiz. Tekh. Poluprovodn.*, 43 (2009), 224.
- [6] SAVRASOV S., SAVRASOV D., *Phys. Rev. B*, 46 (1992), 12181.
- [7] SAVRASOV S.Y., *Phys. Rev. B*, 54 (1996), 6470.
- [8] HOHENBERG P., KOHN W., *Phys. Rev. B*, 136 (1964), 864.
- [9] KOHN W., SHAM L.J., *Phys. Rev. A*, 140 (1965), 1133.
- [10] PERDEW J.P., WANG Y., *Phys. Rev. B*, 46 (1992), 12947.
- [11] BLOCHL P., JEPSEN O., ANDERSEN O.K., *Phys. Rev. B*, 49 (1994), 16223.
- [12] BIRCH F., *J. Geophys. Res.*, 83 (1978), 1257.
- [13] LUO H., GHANDEHAIR K., GEENE R.G., RUOFF A.L., TRAIL S.S., DI SALVO F.J., *Phys. Rev. B*, 52 (1995), 7058.
- [14] KHENATA R., BOUHEMADOU A., HICHOURE M., BALTACHE H., RACHED D., RÉRAT M., *Solid-State Electron.*, 50 (2006), 1382.
- [15] SRIVASTAVA G.P., TÛTÛNCÛ H.M., GÛNHAN N., *Phys. Rev. B*, 70 (2004), 085206.
- [16] GONZALEZ-DIAZ M., RODRIGUEZ-HERNANDEZ P., MUNOZ A., *Phys. Rev. B*, 55 (1997), 14043.

- [17] CHAKRABARTI A., *Phys. Rev. B*, 62 (2000), 1806.
- [18] MUNOZ A., RODRIGUEZ-HERNANDEZ P., MURJICA A., *Phys. Rev. B*, 54 (1996), 11861.
- [19] EL HAJ HASSAN F., AKBARZADEH H., *Comp. Mater. Sci.*, 35 (2006), 423.
- [20] YIM W.M., DISMUKES J.P., STOFKO E.J., POFF R.J., *J. Phys. Chem. Solids*, 33 (1972), 501.
- [21] LEE B.H., *J. Appl. Phys.*, 41 (1970), 2988.
- [22] MC MAHON M.I., NELMES R.J., ALLAN D.R., BELMONTE S.A., BOVOMRATANARAKS T., *Phys. Rev. Lett.*, 80 (1998), 5564.
- [23] KHENATA R., BOUHEMADOU A., SAHNOUN M., RESSHAK A.H., BALTACHE H., RABAH M., *Comp. Mater. Sci.*, 38 (2006), 29.
- [24] CASALI R.A., CHRISTENSEN N.E., *Solid State Commun.*, 108 (1998), 793.
- [25] GANGADHARAN R., JAYALAKSHMI V., KALAISELVI J., MOHAN S., MURUGAN R., PALANIVEL B., *J. Alloy. Compd.*, 5 (2003), 22.
- [26] SMELYANSKY V.I., TSE J.S., *Phys. Rev. B*, 52 (1995), 4658.
- [27] OKOYE C.M.I., *Physica B*, 337 (2003), 1.
- [28] RABAH M., ABBAR B., AL-DOURI Y., BOUHAFS B., SAHRAOUI B., *Mater. Sci. Eng. B-Adv.*, 100 (2003), 163.
- [29] VENGHAUS H., *Phys. Rev. B*, 19 (1979), 3071.
- [30] EL HAJ HASSAN F., AMRANI B., BAHSOUN F., *Physica B*, 391 (2007), 365.
- [31] WANG C.S., KLEIN B.M., *Phys. Rev. B*, 24 (1981), 3393.
- [32] AMBROSCH-DRAXL C., SOFO J.O., *Comput. Phys. Commun.*, 175 (2006), 1.

Received 2015-07-16

Accepted 2015-11-07